Int. J. Electrochem. Sci., 17 **(2022)** Article Number: 220459, doi: 10.20964/2022.04.62

International Journal of
ELECTROCHEMICAL
SCIENCE
www.electrochemsci.org

An Efficient Electrochemical Biosensor Based on Pencil Graphite Electrode Mediated by 2D Functionalized Graphene Oxide to Detect HER2 Breast Cancer Biomarker

Mahdi Sadeghi[1,4], *Soheila Kashanian*[2,1,3,*], *Seyed Morteza Naghib*[4,5,*], *Fateme Haghiralsadat*[6], *Davood Tofighi*[7]

[1] Nanobiotechnology Department, Faculty of Innovative Science and Technology, Razi University, Kermanshah, Iran.
[2] Faculty of Chemistry, Sensor, and Biosensor Research Center (SBRC), Razi University, Kermanshah, Iran.
[3] Nano Drug Delivery Research Center, Health Technology Institute, Kermanshah University of Medical Science, Kermanshah, 6734667149, Iran.
[4] Biomaterials and Tissue Engineering research group, interdisciplinary technologies department, Breast Cancer Research Center (BCRC), Motamed Cancer Institute, ACECR, Tehran, Iran.
[5] Nanotechnology Department, School of Advanced Technologies, Iran University of Science and Technology (IUST), Tehran 1684613114, Iran.
[6] Department of Oral and Maxillofacial Surgery/Oral Pathology, Amsterdam University Medical Centers-location VUMC and Academic Centre for Dentistry Amsterdam (ACTA), Amsterdam Movement Sciences, Amsterdam, The Netherland
[7] Epidemiology, and Research Design Support (BERD), Clinical and Translational Science Center, Department of Psychology and Biostatistics, University of New Mexico, Albuquerque, New Mexico, United States of America
[*]E-mail: kashanian_s@yahoo.com; naghib@iust.ac.ir.

Received: 17 December 2021 / *Accepted:* 20 January 2022 / *Published:* 4 March 2022

Human epidermal growth factor receptor-2 (HER2) tumor marker is a known cancer biomarker and is widely used for diagnosis in clinical BrCa research. In this regard, our team has developed and operated a high selective electrochemical nano-biosensor for detection and quantification of the HER2 biomarker using a pencil graphite electrode mediated by two-dimensional (2D) functionalized graphene oxide (FGO). The unmodified and modified graphite electrodes were evaluated by different techniques, including imaging, spectroscopy, and electrochemistry. When FGO was synthesized by electrochemical oxidation and exfoliation on the graphite electrode surface and its electrochemical performance was measured, the results showed that the modified electrode had a better analytical efficiency. Due to the increase in electrical conductivity and surface area created by FGO on the graphite electrode surface, the sensitivity and electrochemical signal were amplified. The anti-HER2 aptamers were immobilized on the electrode surface through amide bonds, resulting in the binding of carboxyl groups to the FGO and amine groups to the end of the aptamer. Finally, the target HER2 biomarker was recognized. The modified electrode based on electrochemical aptasensing, illustrated a linear response for different concentrations of HER2 biomarker with a linear range from 0.5 ng/mL to 25 ng/mL, with a limit of

detection (LOD) of 0.59 ng/ml without the need for any further amplification. The fabricated nano-biosensor showed good selectivity and stability under experimental conditions that could be used for accurate and rapid detection of HER2 biomarkers. This platform was also used for research and clinical studies, which had relatively good results.

Keywords: graphitic-based aptasensor; HER2 biomarker detection; breast cancer; aptamer; functionalized graphene oxide

1. INTRODUCTION

Breast cancer (BrCa) epidemiology has been steadily expanding throughout the years. Cancer (Ca) is still a major public health problem worldwide and in the United States (U.S.). There are expected to be 281,550 new cases of BrCa and 43,600 deaths from Ca in the U.S. by 2021 [1]. BrCa is a malignant tumor that begins in the breast (Br) cells and spreads uncontrollably. Immunohistochemistry (IHC), an immunoassay-based method, is currently used to detect estrogen (E.R.), progesterone (P.R.), and HER2 receptors in all BrCa tumors to determine the type of BrCa [2]. Br tumors are divided into six intrinsic subtypes contingent on the presence or lack of the three major biomarkers (estrogen (E.R.), progesterone (P.R.), and HER2) [3], basal biomarker (cytokeratin 5/6, epidermal growth factor receptor (EGFR)) [4], and Ki-67 proliferation indicator: luminal A, luminal B, HER2 enriched, normal-like, basal-like, and claudin-low [5-7]. Ki-67 peptide is linked to cell proliferation, with enhanced Ki-67 Expression resulting in a faster rate of cell division. The term "luminal" refers to BrCa that occurs in the luminal (inner) epithelial cells of the Br. The HER2-enriched subtype of BrCa is E.R. and P.R. negative but HER2 positive. This subtype is recognized to grow more quickly and have a worse prognosis than the luminal subtype [8]. Herceptin, on the other hand, is frequently effective in treating HER2-enriched BrCa [9]. The gene expression resemblances between non-epithelial and epithelial cells, as well as adipose tissues, are used to classify typical BrCa [10]. The percentage of tumor cells in normal-like tumor cells is low, and there is no proliferative gene expression [11]. Therefore, early and prompt detection of Ca types should be one of the greatest strategies to prevent an outbreak and serious consequences for medical healthcare. There is an increasing global urgency to develop a point-of-care system for the quick detection of BrCa and other malignancies in order to provide prompt prevention and treatment [12]. As a result, the development of sensitive, selective, and speedy diagnostic equipment is critical in the selection of appropriate treatments and the prevention of Ca [13]. Electrochemical biosensors have evolved as dependable analytical instruments in the recent decade, representing a new promising technique for the detection of many malignancies [14].

Graphene derivatives such as FGO have a crystal lattice adorned with different types of active functional groups (such as epoxy, hydroxyl, carboxylic acid, etc.), which is a good choice for increasing the sensitivity of graphite electrodes. They have not only oxygen-containing functional groups on the surface but also are conducive to expanding the application of FGO. FGO inherits many of the desirable properties of graphene and has more flexible and adjustable properties and greater practical value than graphene owing to their special edge-limiting effects. These honeycomb carbon sheets can lead to quick

electrolyte diffusion and considerably enhance interfacial charge transfer in the middle of the electrode and electrolyte [15]. Furthermore, FGO increases the number of active sites as fast electron transfer routes, which not only increases the active surface of the improved electrode by altering the interface with the electrolyte but also raises the reactivity of the modified electrode [16].

Aptamers are new types of oligonucleotides (or peptides) that can be obtained by in vitro evolution methods. They have the ability to recognize and bind to their complementary target molecules with high selectivity and affinity. Aptamers are widely used in molecular imaging, therapies, diagnostics, and biosensors that imitate antibodies in a variety of applications [17, 18]. Aptamers are more flexible and cost-effective than antibodies because of these features [19].

In this study, we construct an electrochemical aptasensor that can specifically detect changes in the concentration of HER2 biomarker and assess other biomarkers by utilizing the distinctive performance of functionalized graphene oxide material. The biosensing probe (anti-HER2 aptamer) is immobilized on the graphite electrode, resulting in an aptameric-testing device with a readout that can be recorded using a potentiometry reader. Furthermore, differential pulse voltammetry (DPV) demonstrates that the electrochemical signals respond quickly and sensitively by generating a current signal that quickly provides information about the changes due to the presence of FGO. Thus, our findings imply that developed electrochemical biosensing is an effective, quick, low-cost, easy-to-implement, and quantitative method for detecting HER2 and that it may have extensive applications in the analysis of diverse malignancies.

2. EXPERIMENTAL METHODS

2.1. Materials and chemicals.

The pencil graphite type H.B. with a diameter of 2.0 mm was purchased from Owner, Korea. Bovine Serum Albumin (BSA), Human Serum Albumin (HSA), 1-Ethyl-3-(3-Dimethylaminopropyl) Carbodiimide hydrochloride (EDC), and N-HydroxySuccinimide (NHS) was procured from Sigma-Aldrich, USA. Potassium ferricyanide ($k_3Fe(C.N.)_6$) and Potassium ferrocyanide ($K_4Fe(C.N.)_6$) were obtained from Merck, Germany. Anti-HER2 aptamer specifically binds to HER2 biomarker was obtained from Bio Basic Inc, Canada. The sequence of Amine-terminated HER2 DNA aptamer consists of 54-mer oligonucleotide bases is 5′-(NH_2-$(CH_2)_6$-GGG CCG TCG AAC ACG AGC ATG GTG CGT GGA CCT AGG ATG ACC TGA GTA CTG TCC)-3′ [20, 21]. The recombinant human HER2/ErBb2/CD340 biomarker was procured from Sigma-Aldrich, USA. Sulfuric Acid (H_2SO_4 98%), Hydrochloric Acid (HCl 37%), and Ethanol (99.8%) were purchased from Merck, Germany. Other analytical grade reagents were obtained of the top level of purity, and all required aqueous solutions were prepared by double distillation of water.

2.2. Electrochemical measuring equipment and instruments.

All electrochemical measurements, including cyclic voltammetry (CV) and DPV, were performed by using a potentiostat/galvanostat Palmsense BV PGSTAT, with a compliance voltage of 30 V (Echo Chemie, Netherlands) by a three-electrode cell setup. The graphite with various modifications was employed as a working electrode. The desired amplitude of potentials was measured against an Ag/AgCl in a solution containing saturated KCl, acting as the reference electrode. A platinum (Pt) electrode was utilized, functioning as the counter electrode. A freshly polished and prepared electrode was used for each experiment. The measurements were done after applying the three electrodes and immersing them in the probe solution. All electrochemical experiments were implemented in the phosphate-buffered solution (PBS) containing 0.1 M KCl and 5.0 mM $K_4[Fe(C.N.)_6]$ / $K_3[Fe(C.N.)_6]$ (1:1 quota) as ion redox probe couple. The ferri-/ferro-cyanide ionic redox pair in buffered media is frequently employed as a standard probe in electrochemical studies. The $[Fe(C.N.)_6]^{3-/4-}$ ionic redox process involves a single electron transfer and shows quasi-reversible kinetic characteristics with the supposition that the electron transfer in a complete cycle is less resistant [22].

CV curves were determined at a scan rate of 50 mV/s in the range of -0.2 to +0.6 V against Ag/AgCl. DPV was measured between -0.2 to +0.6 V, with an amplitude of 50 mV a pulse width of 0.2 s.

2.3. Pencil-graphite electrode polishing

Prior to analyzing each fabricated aptasensor, a 4 mm pencil-graphite electrode (PGE) was detached with a cutting blade, and the PGE tip was polished with 2000-grit sandpaper until a significant quantity of graphite was separated before being polished on a moistured microfiber cloth. The PGE was cleaned with pure ethanol and then with water before any electrochemical treatment [23].

2.4. Synthesis of functionalized graphene oxide

We used an efficient and novel in situ electrochemical oxidation (Electro-oxidation) technique to directly produce FGO-modified graphite electrodes. Briefly, Cyclic Voltammetry (CV) sweeping the potential from 0.0 to +3.0 V was achieved for a series of four successive sweeps in PBS (pH 6.5) to produce few-layer GONs on the surface of the electrode. [24-26].

2.5. Preparation of the graphite electrode-based aptasensor

To prepare the electrode used in aptasensor, the FGO-modified graphite electrode was incubated in PBS containing 0.20 M EDC and 0.05 M NHS at 8 °C for 80 min to activate the surface of the FGO-modified graphite electrode. This method of binding using the EDC / NHS combination has a wide range of applications. Its uses include: immobilizing peptides and aptamers onto grafted solid surfaces, cross-linking antibodies to functionalized solid support surfaces, and surface functionalizing of gold

nanoparticles with proteins [27]. For covalent conjugation of an activated surface with an amine group (-NH2) of functionalized anti-HER2 aptamer, the FGO-modified electrode was dipped in PBS buffer containing 30 nM anti-HER2 aptamer at room temperature for 1 hour for amide bond formation. Furthermore, Apt/FGO/graphite electrode was immersed in BSA solution with a concentration of 5% at the temperature of 37 ºC under 5% CO_2 atmosphere and humidity with 95% for 5 min to obstruct the activated carboxyl functional moieties on the modified electrode surfaces that are not bound to the amino-functional groups of the anti-HER2 aptamer. The BSA/Apt/FGO-modified graphite electrode was rinsed with PBS several times. Finally, the constructed aptasensor was employed to determine different biomarkers.

2.6. Preparation of solutions

1.44 g Na_2HPO_4, 245 mg KH_2PO_4, 200 mg KCl, and 8.0 g NaCl were combined to make a 1.0 L PBS (0.1 M, pH 7.4). In previously mentioned PBS, a stock solution of aptamer (100 M), HER2, CEA, and HSA was produced and kept at 4°C. In addition, the solution was diluted with PBS to achieve the appropriate concentration. For the Synthesis of FGO, the pH of the 0.1 M PBS was adjusted by 0.01 M HCl.

3. RESULT AND DISCUSSION

3.1. Synthesis and preparation of nanomaterial

We synthesized FGO on the graphite electrode by in-situ electrochemical methods. To produce multi-layers of FGO on the graphite electrode surface, electrochemical oxidation was performed for four sequential sweeps in PBS (pH 6.5) at anodic potentials ranging from 0.0 to +3.0 V. As shown in the CV curves in Fig. 1, electrochemical oxidation of graphite electrodes occurred during the positive sweep at +1.4 V. During the electrochemical oxidation process, the Van der Waals and other cohesive forces in the midst of graphene sheets decreased and then allowed the graphene layers to be separated and spaced apart with the help of gas evolution. As a result, intercalation and exfoliation of graphite to FGO sheets happened. Intercalating compounds comprising a diverse spectrum of hydrophilic oxygenated functional groups were produced, with many of them positioned at the edges of basal planes [28, 29]. The oxygen-containing moieties at the FGO surface or edges significantly influence the electrochemical performance of graphene in respect of the heterogeneous electron transfer rate, which can be useful for better measurement of the target analyte. Accordingly, the number of voltammetric cycles, scan rate, and pH of the supporting electrolyte are among the features that are effective in converting graphite to FGO sheets. This technique is more efficient when performed at modest scan rates and allows adequate time for oxidation and exfoliation of graphene sheets in the graphite structure. Electrochemical techniques are among the least dangerous and cheapest methods for the Synthesis and manufacture of graphene nanomaterials derived from graphite.

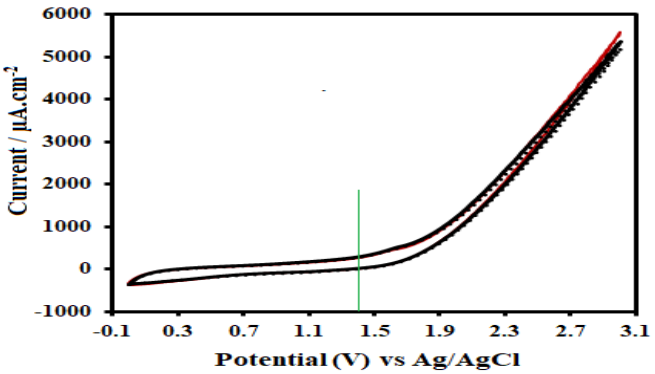

Figure 1. a) CV curves of the Synthesis of FGO on graphite electrode in PBS (pH 6.5).

3.2. Morphology and spectroscopy characterizations

Raman spectroscopy (R.S.), energy-dispersive X-ray spectroscopy (EDS) mapping, and scanning electron microscopy (SEM) was used to analyze as-prepared the FGO sheets. The results indicated that FGO sheets were successfully synthesized.

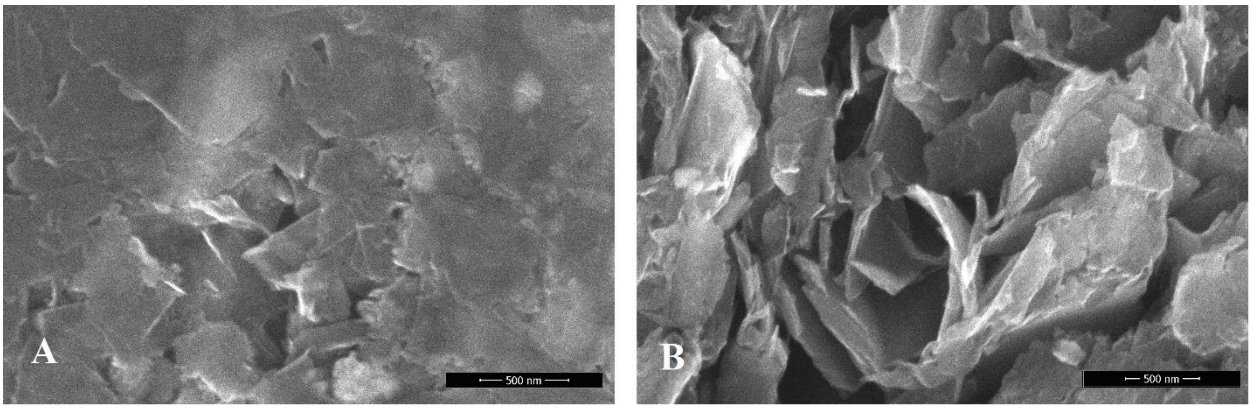

Figure 2. A) SEM image of graphite electrode, B) SEM image of FGO-modified graphite electrode.

The morphology of various bare and modified graphite electrodes was analyzed by SEM. SEM pictures of unmodified and FGO-modified graphite electrodes are shown in Figs. 2 a and b. As illustrated in Fig. 2a, the multi-layer graphitic flakes are closely and firmly stacked and expanded into a two-dimensional structure with large and thin-sized graphitic sheets, indicating that the graphite possessed a platelet-like crystalline form of carbon. In contrast, after in situ successful electrochemical oxidation and exfoliation, a sheet-like structure of FGO layers was evident on the surface of the graphite electrode in Fig. 2b. Under electron beam irradiation, the structure of flake-like FGO reveals a relatively stable nature consisting of a few layers. Thus, the Synthesis of graphene nanomaterials by the electrochemical method has enough energy to prevail over the Van der Waals forces and produces a stable exfoliated graphene

[26]. The produced FGO sheets were properly fixed on the electrode surface, with outstanding stability and durability.

Figs. 3 A and B illustrate the elemental mapping images of oxygen atoms in the unmodified and FGO-modified graphite electrodes, respectively. The amount of oxygenated surface species grows remarkably during the electrochemical oxidation of graphite to FGO.

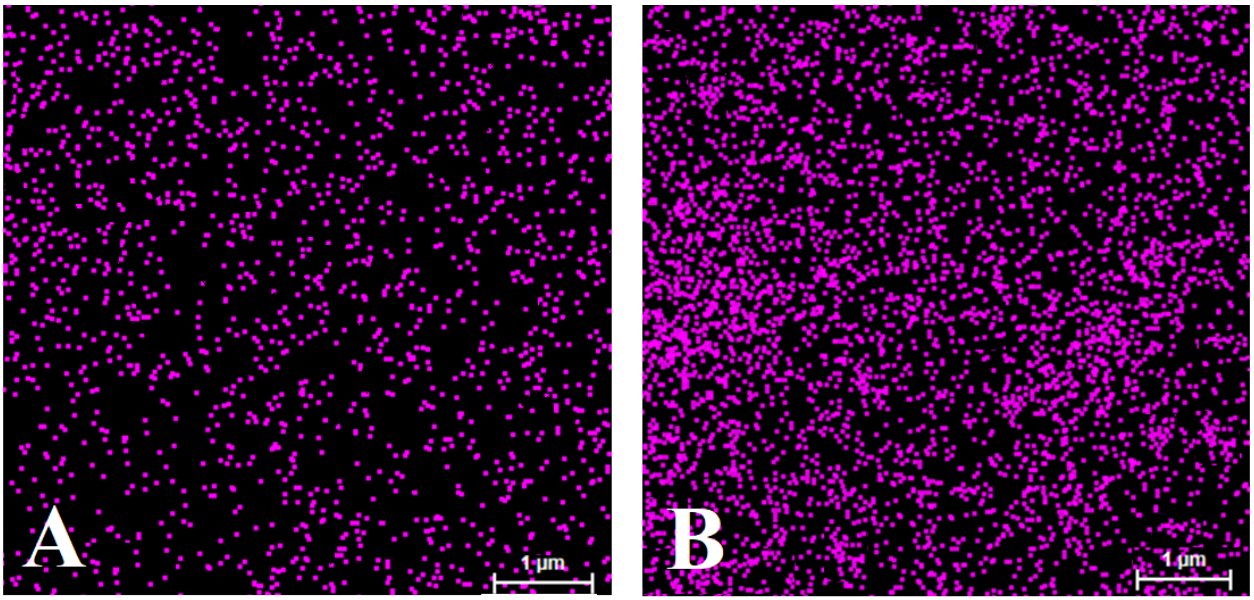

Figure 3. A) EDS mapping scrutiny of the oxygen element on unmodified and B) FGO-modified graphite electrode surface.

The characterization of the unmodified and FGO-modified graphite electrodes was investigated by R.S. R.S. is a useful tool for considering defects and disorders in nanomaterials crystallite structure. Therefore, this technique is practiced in the characterization and confirmation of graphite and its derivatives [30]. Fig. 4 depicts the Raman spectroscopic characterization of graphite and FGO sheets. In general, the Raman spectra of graphite compounds have the main and well-known D and G vibrational bands. The D vibrational band at 1363 cm^{-1} is connected to the formation of local vibration of the sp^3 disorder of the graphene structural band during the oxidation process and species with the mentioned hybridization, which is primarily situated at the margins of graphene flakes. The G sharp vibrational band at 1589 cm^{-1} is also related to the presence of the C-C bond stretching, which is common in all sp^2 carbons. As a result, the intensity of the D and G vibrational bands ratio (I_D / I_G), which reflects the sp^3/sp^2 hybridization carbon ratio, is an influential defining property for the sp^2 domain size in the graphenic structure of carbon, including sp^2 and sp^3 hybridization atoms [31, 32]. The D vibrational band can be noticed at 1363 cm^{-1}, 1360 cm^{-1}, and the G vibrational band at 1589 cm^{-1} and 1599 cm^{-1} for graphite and FGO structure, independently. The D vibrational band in FGO is enlarged because of an abatement in size of the sp^2 domains caused by distortion, vacancies, and defects created during the oxidation process. The presence of oxygenated functional groups causes the G vibrational band in FGO

to shift slightly to a higher wavenumber, resulting in the evolution of the sp^3 hybridized atoms. An increase within the I_D / I_G ratio of FGO to graphite declares the grafting of oxygenated functional groups to graphite planes [33, 34]. Moreover, Raman spectra imaging of carbon compounds includes a familiar 2D vibrational band that reflects the stacking of graphene sheets. When the FGO spectrum is compared to the graphite spectrum, there is a significant difference in their 2D vibrational band. The formation and number of layers of a graphene sheet can be determined using data derived from the shape, intenseness, and position of the 2D vibrating band. The presence of an exceptionally faint 2D vibrational band in the FGO Raman spectra implies that the exfoliated graphene sheets are properly formed [24, 35, 36].

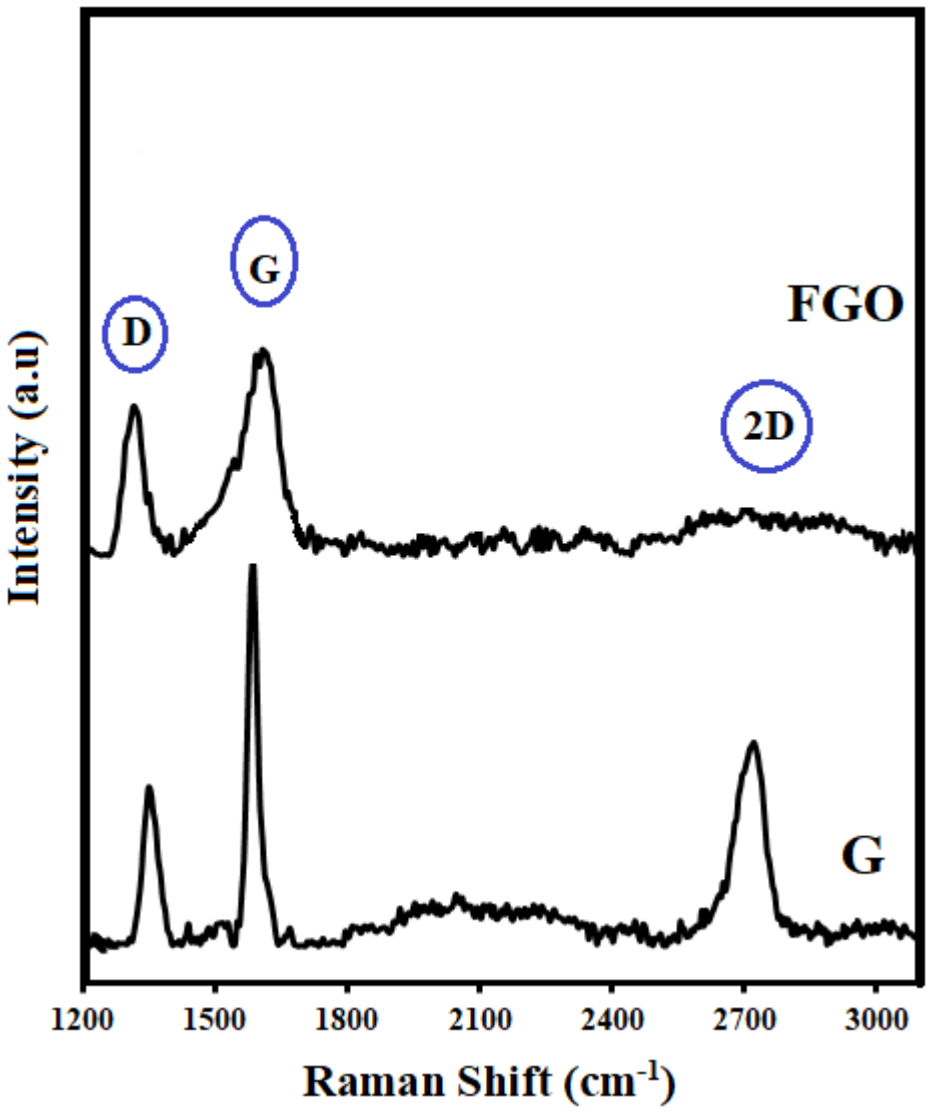

Figure 4. Raman spectra of unmodified (G) and FGO-modified (FGO) graphite electrodes.

3.3. Electrochemical characterization of the synthesized nanomaterial

CV and DPV techniques are the most basic methods used in the development of biosensors and the evaluation of their performance [37]. The CVs of the different graphite electrodes are shown in Fig.

5a. The electrochemical output of the modified graphite electrode was compared with that of the bare graphite electrode. The CV technique is extensively implemented for exploratory purposes. The use of this technique in aptasensor development is common since the CV technique has significant information such as redox processes existing in the analysis and the process reversibility in reactions [38]. Redox peaks in the cyclic voltammogram correlated with the oxidation of ferrocyanide ion and reduction of ferricyanide ion on the graphite electrode surface were seen at 0.28 and 0.19 V, independently. The peak current densities for the FGO-modified graphite electrode were appreciably higher than those of the unmodified graphite electrode. This amplification in electrochemical signal could be attributed to the increased conductivity in the presence of the graphene sheets and enhanced diffusive mass transport of the anion $[Fe(C.N.)_6]^{4-}$ reactant to the FGO/graphite electrode surface when compared to the unmodified graphite electrode. All electrochemical characterizations of the prepared graphite electrodes were carried out in PBS containing the 5.0 mM Potassium ferri-/ferro-cyanide (+ 0.1 M KCl) as a standard electrochemical probe solution.

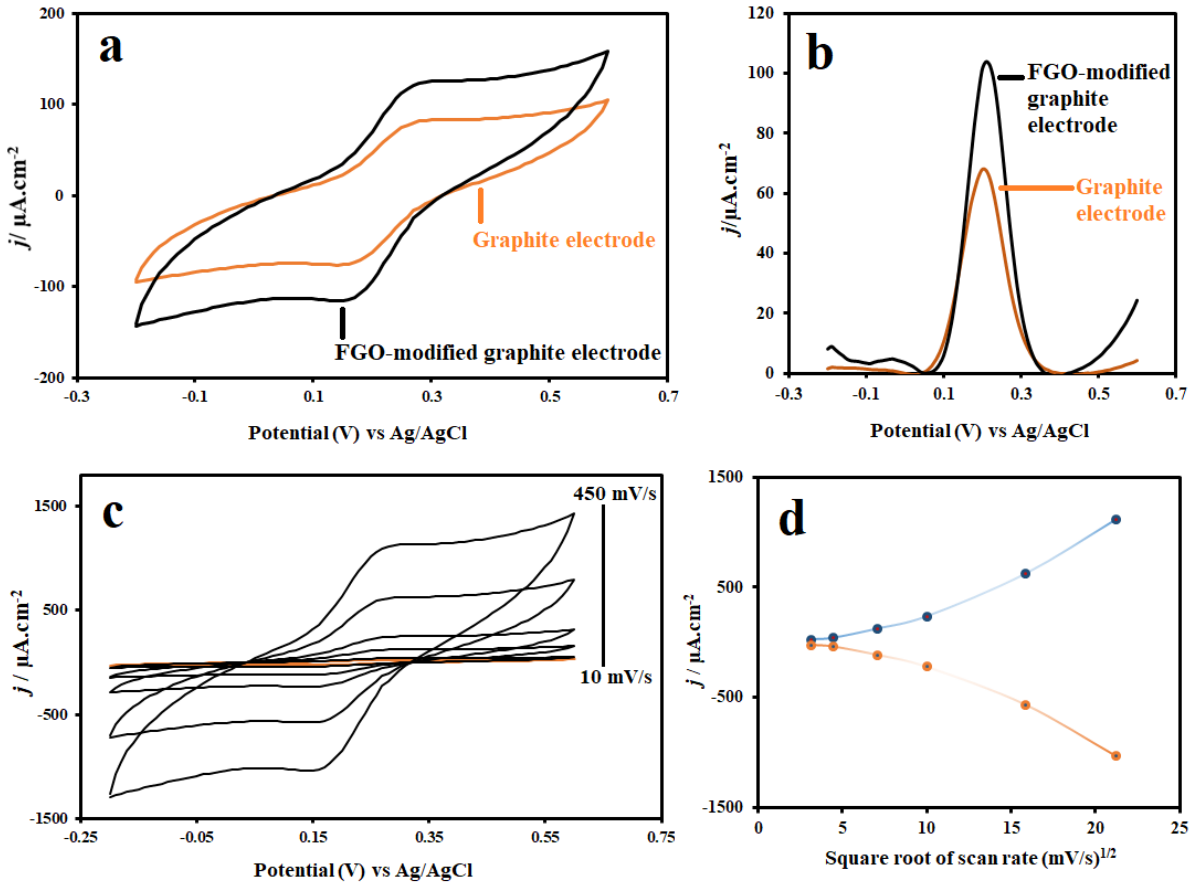

Figure 5. a) C.V.s of unmodified and FGO-modified graphite electrodes at a scan rate of 50 mVs^{-1}, b) DPV curves of unmodified and FGO-modified graphite electrodes, c) CV graphs characterization of FGO-modified graphite electrode based on various scan rates of 10, 20, 50, 100, 250, and 450 mVs^{-1}, all experiment analysis carried out in PBS containing 5.0 mM ferri-/ Ferro-cyanide (1:1) ion redox as an electrochemical probe, d) The curves of the redox peaks current density against the square root of the scan rate based on C.V.s characterization of rGONs-modified graphite electrode.

The differential pulse voltammograms of the unmodified and modified graphite electrodes are shown in Fig. 5b. After modifying the electrode with FGO sheets, the peak current increased significantly. Electrochemical methods based on the pulse techniques like DPV are more sensitive than the linear sweep systems due to the minimalization of the interfering capacitive current. The pulse procedure is mostly employed for quantifying measurements since this technique has a significantly larger detection limit than other well-known electrochemical techniques due to a greater signal-to-noise ratio.

Fig. 5c demonstrates the peak currents in cyclic voltammogram for redox states in the presence of standard electrochemical probes at the scan rates from 10 - 450 mV/s. There is a relationship of linearity between the square root of the sweep rate against the redox of peak current density (Fig. 5d). When the scan rate increases, the anodic and cathodic peak current densities are elevated significantly at the same time, indicating that the diffusion-controlled is the result of the investigated redox reaction [39]. According to the results, the FGO-modified graphite electrode was very stable and reproducible.

3.4. Optimization and immobilization of anti-HER2 aptamer on the modified electrode

The predicted secondary structure of the anti-HER2 aptameric strand shows double stem-loops, and a random sequence is situated within the structure of its primary stem-loop, anticipated to be bound to the particular place of HER2 biomarker. The transducer layer is extremely important for immobilization of the aptamer strand and, finally, stabilization of the formed G-quadruplex, in addition to affecting the sensitivity and selectivity of the aptasensor. It seems that nanomaterials are ideal platforms for immobilization of anti-HER2 aptamer strands due to their privileged biocompatibility as well as the extremely large surface area to volume ratio [20]. The interaction between HER2 biomarker and anti-HER2 aptameric strand led to opening the anti-HER2 hairpin duplex and the formation of HER2 biomarker and anti-HER2 aptamer complex (Tabasi et al. 2017). Moreover, aptamers are insulating compounds that the phosphate moieties in their structures would be ionized to many negative charges in an aqueous solution that barricade the transfer of electrons on the surface of the electrode by reason of the intense electrostatic expulsion through ferri-/ferro-cyanide ionic redox available in electrochemical probe [40]. As a result, a remarkable decrease in CV and DPV peak current measurements in aptasensor was observed. The difference of electrochemical current density obtained by changing biomarker concentration was used compared to the BSA stabilization step as the measurement system, which is displayed as Δj. The effect of two important experimental parameters, i.e., anti-HER2 aptamer concentration and incubation binding time for HER2 biomarker, were explored. In the first step, the carboxyl moieties on the FGO-modified graphite electrode surface were stimulated by immersing the electrodes in EDC/NHS solution. EDC is the most desired cross-linker for biochemical conjugations considering it can effectively construct conjugates and bonds in the middle of two peptide molecules, among proteins and oligonucleotides, or different molecules and structures that have carboxyl and amine, functional groups. EDC cross-linking formalities often include the NHS, which promotes coupling efficiencies as well as greater stability of amine-reactive mediators. EDC, in combination with the NHS, enables the two-step coupling of two peptides without affecting the carboxyls of the second peptide or

any other construction. EDC stimulates carboxyl moieties and creates an amine-reactive O-acylisourea intermediate that automatically reacts with early amines to create an amide bond and an isourea corollary. The O-acylisourea intermediate is unstable in aqueous solutions, and failure to react with an amine will cause hydrolysis of the intermediate, restoration of the carboxyls, and liberating of N-substituted urea. EDC couples NHS to carboxyls, which creates an NHS ester that is substantially more greatly stable than the O-acylisourea intermediate and permits for effectual conjugation to primary amines at physiological pH [41, 42]. Next, FGO-modified graphite electrodes were placed in different concentrations of aptamer (10, 15, 30, 45, 50, and 70 nM). In the third step, the Apt/FGO-modified electrodes were immersed in 5% BSA solution and finally incubated with 200 ng/ml HER2 solution. As the anti-HER2 aptamer concentration increased to 30 nM, the current density also increased. However, no significant change was seen for aptamer concentration greater than 30 nM since the modified surface of the electrode was thoroughly saturated with anti-HER2 aptamer [43]. Accordingly, a concentration of 30 nM anti-HER2 aptamer was selected as the ideal concentration. Following, to gain the most effective incubation binding time of the HER2 biomarker, the aptasensor for 10, 20, 30, 40, 60, and 90 min in 200 ng/mL of HER2 was incubated. The intensity of current density (*j*) raised together with increasing the incubation binding time and then stayed almost steady after 30 min incubation because the surface of the electrode was saturated. For this reason, the most favorable incubation time was determined to be 30 min.

3.5. Sensing performance of aptasensor toward HER2 biomarker

Since the selected anti-HER2 aptamer strand is established from 54 oligonucleotide bases, optimizing the connective layer for biosensor to bind the anti-HER2 aptamer strand and immobilize the generated G-quadruplex from the anti-HER2 aptamer, is especially important. Given their high affinity and intrinsic compatibility, FGO sheets could be used as a platform for immobilizing aptamer strands, pursued by HER2 biomarker recognition via G-quadruplex formation among aptamer strands and HER2. Therefore, the aptasensor based on BSA/Apt/FGO-modified graphite electrodes, were employed to evaluate each stage of the detection procedure of various biomarkers.

The proposed aptasensor was also employed to detect HER2 biomarkers at various doses. For this purpose, it was tested at concentrations ranging from 0.5 to 300 ng/mL HER2, and then, the interaction results were measured using the DPV technique (Fig. 6a). As demonstrated in Fig. 6b, the current density increases as the concentration of HER2 increases. The electrochemical response of the aptasensor towards HER2 is good linearity withinthe concentration range of 0.5 to 300 ng/ml, with a LOD of 0.59 ng/mL. The linear relationship between Δj and Log [C_{HER2}] were: Δj ($\mu A.cm^{-2}$) = 21.56 + 24.57 Log [C_{HER2}] (ng/ml) and an R^2 of 0.9894, where [C_{HER2}] is the concentration of HER2 biomarker. The limit of quantification (LOQ) were obtained to be 1.78 ng/mL. Thus, this aptasensor provides acceptable and satisfactory performance. The significant stability of the platform can be ascribed to the MPA/FGO/graphite electrode and strong covalent binding of anti-HER2 aptamer to the FGO-modified graphite electrode via amide bonding. Therefore, the results indicate good performance even at lower

HER2 biomarker concentrations, and the developed platform can be employed to monitor small changes in biomarker concentration in many forms of cancer during the primary stage of the disease.

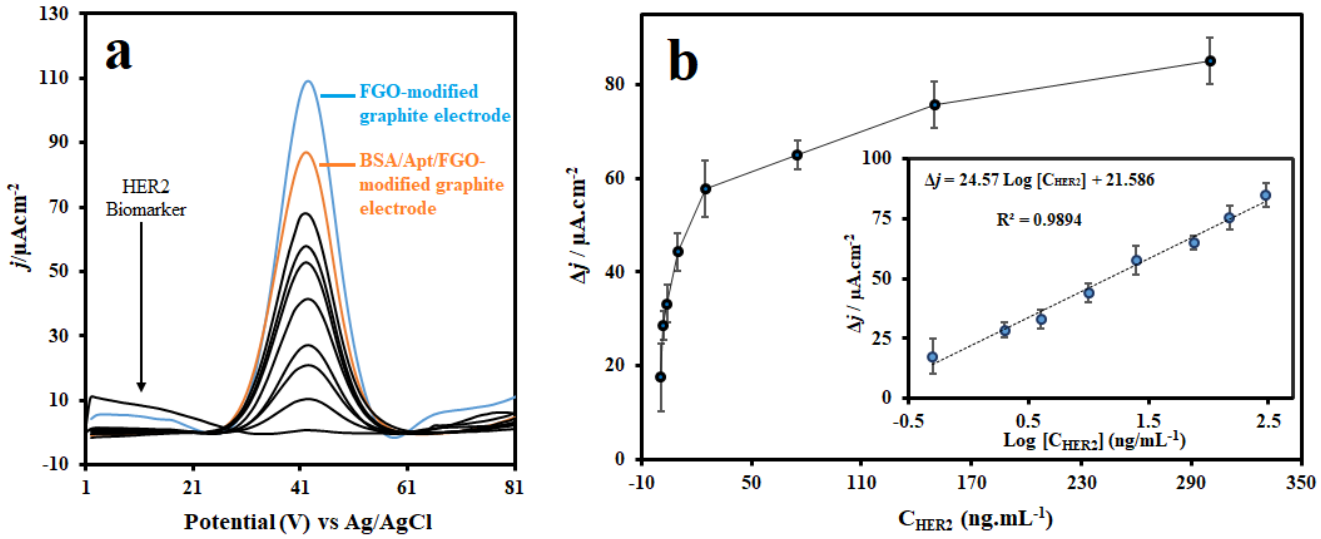

Figure 6. a) DPV responses of the nano-biosensor with diverse concentrations of HER2 biomarkers (0.5, 2, 4, 10, 25, 75, 150, and 300 ng/mL), b) Dependence of current density on logarithm of HER2 biomarker concentration (inset: the linear portion of calibration curve).

The selectivity of electrochemical nano-biosensor was also investigated using different interfering agents, such as carcinoembryonic antigen (CEA) and Human Serum Albumin (HSA). The results showed that CEA and HSA only had a minor change in current density (Fig. 7), whereas the HER2 biomarker had a significant change. This result implies that the developed nano-biosensor has a high level of reliability and efficiency.

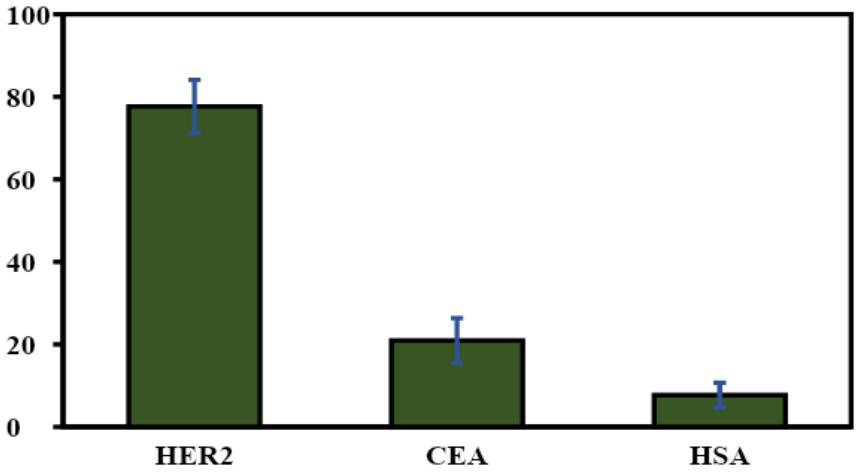

Figure 7. Selectivity of aptasensor in presence of 100 ng/mL HER2, CEA, and HAS

3.6. Real sample analysis

The clinical application of the fabricated aptasensor for HER2 biomarker was analyzed in patients' serum samples, provided by Motamed Breast Cancer Research Institute. The aptasensor was employed for detection and quantification of HER2 biomarker in the serum samples. The test outcomes are shown in Table 1 and compared to the ELISA report. The results show that the proposed aptasensor has acceptable reliability and sensitivity for clinical applications.

Table 1. HER2 biomarker analysis in human serum samples

Serum Sample no.	Concentration ($ng.mL^{-1}$)		RSD (٪)	*P*-value
	Proposed aptasensor	ELISA Kit		
1	**33.6 ± 0.34**	**23.4 ± 0.23**	**3.9**	**<0.05**
2	**49.5 ± 0.44**	**42.7 ± 0.29**	**2.4**	**0.63**
3	**87.8 ± 0.24**	**81.4 ± 0.20**	**1.9**	**0.049 (<0.05)**
4	**99.5 ± 0.71**	**88.8 ± 0.81**	**4.2**	**0.69**
The results are the average of four independent measurements ± standard error.				

4. CONCLUSION

A novel and well-organized nano-biosensor was exploited for detection and quantification of the HER2 biomarker. By increasing conductivity and specific surface area, FGO sheets can improve electrochemical signal and sensitivity. Furthermore, significant covalent bonds between the aptamer strand and HER2, improved the stability of the generated G-quadruplex. Nano-biosensor fabrication yielded a LOD value of 0.59 ng/mL for HER2. The findings of this study support the aptasensor's effective performance. The developed electrochemical aptasensor can be used as an efficient platform to detect and monitor a wide range of cancer biomarkers.

References

1. R. L. Siegel, K. D. Miller, H. E. Fuchs and A. Jemal, *CA: Cancer J. Clin*., 71 (2021) 7.
2. C. S. Vallejos, H. L. Gómez, W. R. Cruz, J. A. Pinto, R. R. Dyer, R. Velarde, J. F. Suazo, S. P. Neciosup, M. León, M. A. de la Cruz and C. E. Vigil, *Clin. Breast Cancer*, 10 (2010) 294.
3. C. M. Perou, T. Sørlie, M. B. Eisen, M. Rijn, S. S. Jeffrey, C. A. Rees, J. R. Pollack, D. T. Ross, H. Johnsen, L. A. Akslen, Ø. Fluge, A. Pergamenschikov, C. Williams, S. X. Zhu, P. E. Lønning, A. Børresen-Dale, P. O. Brown and D. Botstein, *Nature*, 406 (2000) 747.
4. D. M. Abd El-Rehim, S. E. Pinder, C. E. Paish, J. Bell, RW. Blamey, J. FR. Robertson, Robert I. Nicholson and Ian O. Ellis, *J. Pathol*., 203 (2004) 661.
5. A. Urruticoechea, I. E. Smith and M. Dowsett, *Clin. Oncol*., 23 (2005) 7212.
6. J. Rhee, S. –W. Han, D. -Y. Oh, J. H. Kim, S. -A. Im, W. Han, I. A. Park, D. –Y. Noh, Y. –J. Bang and T. -Y. Kim, *BMC cancer*, 8 (2008) 1.
7. B. Keam, S. –A. Im, K. –H. Lee, S. –W. Han, D. –Y. Oh, J. H. Kim, S. –H. Lee, W. Han, D. –W. Kim, T.-Y. Kim, I. A. Park, D. –Y. Noh, D. S. Heo and Y. –J. Bang, *Breast Cancer Res*., 13 (2011) 1.

8. S. M. Fragomeni, A. Sciallis and J.S. Jeruss, *Surg. Oncol. Clin*., 27 (2018) 95.
9. D. Slamon, W. Eiermann, N. Robert, T. Pienkowski, M. Martin, M. Press, J. Mackey, J. Glaspy, A. Chan, M. Pawlicki, T. Pinter, V. Valero, M. –C. Liu, G. Sauter, G. Minckwitz, F. Visco, V. Bee, M. Buyse, B. Bendahmane, I. Tabah-Fisch, M. –A. Lindsay, A. Riva and J. Crown, *N. Engl. J. Med*., 365 (2011) 1273.
10. L. Hinck and I. Näthke, *Curr. Opin. Cell Biol*., 26 (2014) 87.
11. O. Yersal and S. Barutca, *World J. Clin. Oncol*., 5 (2014) 412.
12. L. Syedmoradi, M. L. Norton and K. Omidfar, *Talanta*, 225 (2021) 122002.
13. L.Suresh, J. Bondili and P. Brahman, *Mater. Today Chem*., 16 (2020) 100257.
14. P. S. Pakchin, M. Fathi, H. Ghanbari, R. Saber and Y. Omidi, *Biosens. Bioelectron*., 153 (2020) 112029.
15. D. Chen, H. Feng, and J. Li, *Chem. Rev*., 112 (2012) 6027.
16. S. A. Hashemi, S. M. Mousavi, S, Bahrani, S. Ramakrishna, A. Babapoor and W. –H. Chiang, *Anal. Chim. Acta*, 1107 (2020) 183.
17. A.-E. Radi, *Int. J. Electrochem.*, (2011) 863196
18. G. Figueroa-Miranda, L. Feng, S. C. –C. Shiu, R. M. Dirkzwager, Y. –W. Cheung, J. A. Tanner, M. J. Schöning, A. Offenhäusser and D. Mayer, *Sens. Actuators B Chem*., 255 (2018) 235.
19. C. A. L. Espiritu, C. C. Justo, M. J. Rubio, M. Svobodova, A. S. Bashammakh, A. O. Alyoubi, W. L. Rivera, A. P. Rollon and C. K. O'Sullivan**,** *ACS Infect. Dis*., 4 (2018)1306.
20. C. Gu, C. Guo, Z. Li, M. Wang, N. Zhou, L. He, Z. Zhang and M. Du, *Biosens. Bioelectron*., 134 (2019) 8.
21. J. H. Niazi, S. K. Verma, S. Niazi and A. Qureshi, *Analyst*, 140 (2015) 243.
22. A. Varyambath, C. H. Tran Wen, L. Song and I. Kim, *ACS omega*, 2 (2017) 7506.
23. J. Kariuki, E. Ervin and C. Olafson, *Sensors*, 15 (2015) 18887.
24. F. Zeng , Z. Sun, X. Sang, D. Diamond, K. T. Lau and X. Liu, *ChemSusChem*, 4 (2011) 1587.
25. S. Rabieh, A. Koushanpour and F. Tajabadi, *Electroanalysis*, 27 (2015) 2377.
26. H.-L. Guo, X. –F. Wang, Q. –Y. Qian, F. –B. Wang and X. –H. Xia, ACS nano, 3 (2009) 2653.
27. M.P. Wickramathilaka and B.Y. Tao, *J. Biol. Eng*., 13 (2019) 1.
28. F. Liu, C. Wang, X. Sui, M. A. Riaz, M. Xu, L. Wei and Y. Chen, *Carbon Energy*, 1 (2019) 173.
29. W. Yu, L. Sisi, Y. Haiyan and L. Jie, *RSC Adv*., 10 (2020) 15328.
30. P. Selvarajan, G. Chandra, S. Bhattacharya, S. Sil, A. Vinu and S. Umapathy, Emergent *Mater.*, 2 (2019) 417.
31. F. Catania, E. Marras, M. Giorcelli, P. Jagdale, L. Lavagna, A. Tagliaferro and M. Bartoli, *Appl. Sci*., 11 (2021) 614.
32. E. F. Sheka, Y. A. Golubev and N .A. Popova, *Nanomaterials*, 10 (2020) 2021.
33. M. P. Lavin-Lopez, A. Paton-Carrero, L. Sanchez-Silva, J. L. Valverde and A. Romero, *Adv. Powder Technol*., 28 (2017) 3195.
34. S. Perumbilavil, P. Sankar, T. P. Rose and R. Philip, *Appl. Phys. Lett*., 107 (2015) 051104.
35. J. –B. Wu, M. –L. Lin, X. Cong, H. –N. Liu and P. –H. Tan, *Chem. Soc. Rev*., 47 (2018) 1822.
36. A. Jorio, and R. Saito, *Int. J. Appl. Phys*., 129 (2021) 021102.
37. L. C. Brazaca, L. Ribovski, B. C. Janegitz and V. Zucolotto, *Medical Biosensors for Point of Care (POC) Applications*, (2017) 229.
38. C. Karunakaran, R. Rajkumar and K. Bhargava, *Biosensor and Bioelectron*ics, Chapter 1 - Introduction to Biosensors, Editor(s): Chandran Karunakaran, Kalpana Bhargava, Robson Benjamin, Biosensors and Bioelectronics, Elsevier, 2015, Pages 1-68,
39. Y. Dai, K. Abbasi, M. DePietro, S. Butler and C. C. Liu, *Sci. Rep*., 8 (2018) 1.
40. Z. Wang, P. Dong, Z. Sun, C. Sun, H. Bu, J. Han, S. Chen and G. Xie, *J. Mater. Chem. B.*, 6 (2018) 2426.
41. W. Eck, G. Craig, A. Sigdel, G. Ritter, L. J. Old, L. Tang, M. F. Brennan, P. J. Allen and M. D. Mason, *ACS nano*, 2 (2008) 2263.

42. N. Reddy, R. Reddy and Q. Jiang, *Trends Biotechnol.*, 33 (2015) 362.
43. Y. Zhu, P. Chandra and Y. -B. Shim, *Anal. Chem.*, 85 (2013)1058.